Bralower, T.J., Premoli Silva, I., and Malone, M.J. (Eds.)
Proceedings of the Ocean Drilling Program, Scientific Results Volume 198

18. Petrography and Correlation of Cenozoic Ash Layers Recovered on Shatsky Rise, ODP Leg 198[1]

Kyle L. Gadley[2,3] and Kathleen M. Marsaglia[2]

ABSTRACT

In this study of volcanic ash retrieved from Shatsky Rise during Ocean Drilling Program Leg 198, the texture and composition of the volcanic components (glass and crystals) were used to fingerprint ash layers for detailed correlation. Correlations among ash layers in holes drilled at the same site as well as between sites, including sites on different parts (highs) of the rise, were tested. Although high-to-high correlations failed, intrahigh correlations were more successful. Our data suggest a significantly different source for some pyroclastic debris, especially at Site 1208, possibly associated with pumice rafts carried northward from the Izu-Bonin arc by the Kuroshio Current. Other ashes are consistent with rhyolitic to dacitic air fall ash from Asian arc volcanoes. We were not able to texturally distinguish between air fall ash and pumice-raft fallout but suspect that the latter is associated with higher percentages of vesiculated ash components, as we demonstrate occur in more proximal Izu-Bonin pyroclastic deposits.

INTRODUCTION

Shatsky Rise is a Mesozoic large igneous province in the west central Pacific Basin east of Japan, which is the approximate length (1300 km) of the state of California (Sliter and Brown, 1993). Three major topographic highs, the largest being Shatsky Plateau, compose Shatsky Rise (Fig. F1). Sediments found on Shatsky Rise range from Cretaceous to Pleistocene in age and are at relatively shallow burial depths (Sliter and

F1. Leg 198 site location map, p. 10.

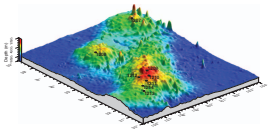

[1]Gadley, K.L., and Marsaglia, K.M., 2005. Petrography and correlation of Cenozoic ash layers recovered on Shatsky Rise, ODP Leg 198. *In* Bralower, T.J., Premoli Silva, I., and Malone, M.J. (Eds.), *Proc. ODP, Sci. Results,* 198, 1–26 [Online]. Available from World Wide Web: <http://www-odp.tamu.edu/publications/198_SR/VOLUME/CHAPTERS/108.PDF>. [Cited YYYY-MM-DD]
[2]Department of Geological Sciences, California State University Northridge, 18111 Nordhoff Street, Northridge CA 91330-8266, USA. Correspondence author: **kathie.marsaglia@csun.edu**
[3]Current address: Weston Solutions, Inc., 14724 Ventura Blvd., Suite 100, Sherman Oaks CA 91403, USA.

Initial receipt: 1 March 2004
Acceptance: 27 January 2005
Web publication: 19 August 2005
Ms 198SR-108

Brown, 1993). Shatsky Rise has been the focus of eight Deep Sea Drilling Project (DSDP) and Ocean Drilling Program (ODP) drilling expeditions. Pleistocene to Miocene sediments were recovered at DSDP Sites 47, 48, 50, 305, 306, and 577 and ODP Site 810 on the southern plateau. Drilling during Leg 198 (Fig. F1) penetrated the Northern (Site 1207) and Central (Site 1208) Highs of Shatsky Rise in addition to the larger Southern High (Sites 1209–1214). The Cenozoic sections recovered at all of these sites except Site 1214 were ash bearing, and most sections contained rafted pumice fragments (Bralower, Premoli Silva, Malone, et al., 2002).

The ash record of Shatsky Rise is concentrated in the post-2.6-Ma section that accumulated during a period of global cooling. This increase in explosive volcanic activity at ~2.6 Ma has been noted around the globe and tentatively linked to the onset of Northern Hemisphere glaciation (e.g., Kennett, 1977; Kennett et al., 1977; Bray, 1974, 1979; Prueher and Rea, 1998). Furthermore, Natland (1993) suggested that ash frequency may be linked to changes in dispersal associated with jet stream migration.

The best ash record recovered during Leg 198 was at Site 1208, where there are a few ash layers in the upper Miocene section and a maximum at ~2.6 Ma (Cores 198-1208A-13H and 14H). This site contains more discrete ash layers (20 total) than the previous Shatsky record set at Site 810 (12). Site 1208 is also unique in that it contains a thicker than expected upper Cenozoic section that is attributable to the presence of sediment drift deposits (Bralower, Premoli Silva, Malone, et al., 2002). It is not known how sediment reworking on the Central High may have modified the ash record. Elsewhere on Shatsky Rise at other Leg 198 and previous DSDP sites, incomplete ash records may be attributed to the erosive effects of deep ocean currents. Prueher and Rea (1998) did not use Site 884 for their tephrochronolgy work because it is in the Meiji Drift. Therefore the ash record may provide some insight into drift sedimentation processes and dynamics across Shatsky Rise.

Natland (1993) analyzed ash beds and pumice fragments from Site 810 on Shatsky Rise located near Site 1212. Although Natland collected geochemical data, he did not attempt to correlate the ashes based on their geochemical signatures. Indeed, he used age models based on magnetostratigraphy to correlate the ashes from Site 810 on Shatsky Rise to DSDP Sites 578–580, which lie ~1000–1500 km to the east and northeast. Ash geochemistry, age relationships, and considerations of atmospheric and ocean currents led Natland (1993) to conclude that the source of the ash was most likely to the north, namely arc volcanoes along the Kurile and northern Japan margins. Natland (1993) described the vitric ash components as being colorless (rhyolitic) and tan/brown (andesitic). He did not attempt to correlate the Site 810 ashes to the few ash beds recovered at other DSDP sites on Shatsky Rise.

Shipboard smear slide analyses of the Leg 198 ashes indicated that they were compositionally variable, containing a variety of glass textures and mineral constituents (Bralower, Premoli Silva, Malone, et al., 2002). This study is designed to test whether detailed compositional modes can be used to "fingerprint" individual ash beds for correlation and serve as an alternative to geochemical analysis. Our hypothesis was that the proportions of various vitric (subdivided by morphology/texture) and mineral components can be used as a correlation tool to help correlate the ash record from north to south across Shatsky Rise.

METHODS

A total of 58 samples of unconsolidated ash were collected for this study (Table T1; Fig. F2): 3 from Hole 1207A, 18 from Hole 1208A, 5 from Hole 1209A, 8 from Hole 1209B, 7 from Hole 1210A, 1 from Hole 1210B, 1 from Hole 1211A, 2 from 1211B, 5 from 1212A, 6 from 1212B, and 2 from Hole 1213A. The samples were acquired during the leg and on a subsequent trip to the Gulf Coast Core Repository at Texas A&M University in College Station, Texas. Each sample was first air-dried and then dry sieved to separate the sand-sized fraction (0.063–2 mm) from finer (<0.063 mm) material. Several of the collected samples were very fine and contained no sand-sized fraction (Table T1). Sand fractions for 41 of the samples were then epoxied to glass slides and ground to a thickness of 30 µm. Thin sections were etched with hydrofluoric acid and stained using the procedure outlined by Marsaglia and Tazaki (1992). The staining served to differentiate Ca from K feldspar, but other siliceous components also stain. Thus, this technique provides information on the Ca and K content of vitric components as well.

Point-count categories included mineral grains (crystals) and glass fragments, subdivided by texture/morphology, degree of vesicularity, and composition (color/stain) (summarized in Table T2). Much of the description and interpretation of shard morphology has been based on observations of ash using a scanning electron microscope (e.g., Heiken and Wohletz, 1985). In thin section, the 30 µm thickness provides some idea of the three-dimensionality of the textures we describe but, in essence, we are dealing with two-dimensional slices or views. Therefore, we devised a classification scheme (Fig. F3) that makes use of our two-dimensional slices of three-dimensional fragments and allows us to expand on the cuspate, platy, and pumice shard textures outlined by Fisher and Schmincke (1984).

An automated-stage point-counting system attached to a petrographic microscope was used to determine compositional modes from the thin sections. A total of 400 points were counted on each section using the Gazzi-Dickinson method (Dickinson, 1970; Ingersoll et al., 1984); bioclasts were noted but were not included in the 400-point total. Raw point count data are presented in Table T1 and were recalculated in an Excel spreadsheet program using the parameters listed in Table T2. Recalculated parameters are listed in Table T3 and plotted in Figures F4, F5, F6, and F7. In cases where the volcanic material was of insufficient quality or quantity to count 400 grains, the volcanic components in the samples were qualitatively described (Table T1). Age is an important parameter in ash bed correlation. To facilitate ash bed correlation, the ages of Leg 198 ash beds were estimated using two different methods (Table T1). The first method extrapolated ages from age-depth plots created by shipboard scientists using biostratigraphic (nannofossil and foraminiferal) datums (Bralower, Premoli Silva, Malone, et al., 2002). The second method extrapolated ages from shipboard paleomagnetic data as interpreted by Bralower, Premoli Silva, Malone, et al. (2002) and postcruise data (H. Evans, pers. comm., 2005) according to the geomagnetic polarity timescale of Cande and Kent (1995). As Natland (1993) points out, linear interpolations of age using such methods require a constant rate of sedimentation and lack of vertical core distortion. We used these data to target likely correlative pairs of ash beds from different holes or sites. Then, for each ternary plot, the minimum percent difference (any of the three parameters) between the two ash

T1. Sample intervals and age estimates, p. 20.

F2. Stratigraphic columns and ash layer occurrence, p. 11.

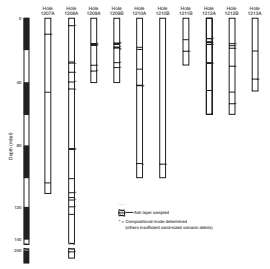

T2. Counted and recalculated parameters, p. 21.

F3. Pyroclast classification scheme, p. 12.

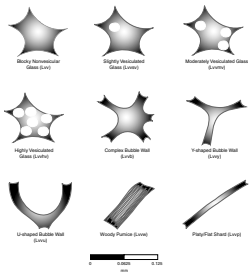

T3. Recalculated parameters, p. 23.

F4. Colorless glass components, p. 13.

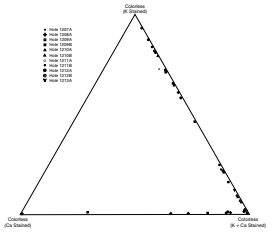

F5. Vesiculated vs. shards vs. blocky texture plots, p. 14.

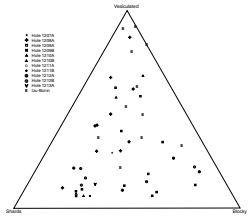

samples was entered into a correlation table (Fig. F8, Table T4). An average minimum percent difference was calculated based on the number of ternary plots used in each case (number changes because some ash beds do not contain all glass stain types). This number ("Total percentage" in Table T4) provides a means to evaluate the likelihood of correlation. The correlations were quantified as being excellent (0%–3%), good (3%–5%), moderate (5%–8%), or poor (>8%). We also used this method to test the similarity of ash beds that were not time-correlative.

Additional data were collected from marine tephras recovered from the Izu-Bonin intraoceanic arc during ODP Leg 126. The samples were previously described in Marsaglia (1992). For this study, selected samples from Leg 126 were recounted using the same ash classification scheme used for the Leg 198 samples (Fig. F3). In the Leg 126 samples, a total of 300 points (vitric components) were counted instead of the 400-point total counted in the Leg 198 samples owing to lower vitric to crystal ratios in the Leg 126 samples (Table T1). The data were recalculated using the parameters in Table T2.

RESULTS

Compositional/Textural Modes

The point-count data presented in Table T1 indicate that the ash recovered from Shatsky Rise during Leg 198 consists of predominantly colorless glass exhibiting a range from blocky to bubble-wall to pumice textures (e.g., Fig. F3) and lesser amounts of crystal phases. Plagioclase is the dominant crystal component in these ashes, ranging as high as 12% of the total composition but averaging <3%. Traces (<2%) of quartz, pyroxene, amphibole, biotite, and K-feldspar were also noted. The dominant components are colorless vitric pyroclasts, but as much as 5% of the vitric components exhibit tan, brown, or black groundmass. In turn, these darker fragments are generally nonvesicular and blocky (Lvv) (Fig. F3), which, coupled with their color, suggests that they are mafic to intermediate in composition. The colorless glassy fragments were classified according to their stain and texture/morphology including degree of vesicularity (Fig. F3). They were mostly either K stained or exhibited both Ca and K stain, but in a few samples the glass is predominantly Ca stained. The relative proportions of Ca- and K-stained samples are shown in the ternary plot in Figure F4. The few unstained colorless fragments noted in Table T1 may have been completely embedded in protective epoxy that prohibited their staining.

The vitric clast classification scheme (Fig. F3) is based on variations in shard shape and degree of vesicularity of glass, ranging from nonvesicular to highly vesiculated pumice. We observed a wide assortment of vitric grain assemblages within the samples, so several schemes of recalculated parameters (Tables T2, T3) were devised to illustrate the textural variability of the ash beds. From these, ternary plots showing relative proportions of ash texture were constructed (e.g., vesiculated vs. shards vs. blocky pyroclasts; slightly/moderate vesiculated vs. highly vesiculated/pumice vs. shards; and U-shaped bubble wall vs. Y-shaped bubble wall vs. platy shards) (Figs. F5, F6, F7). Plots for the subsets of shard populations according to stain (K, Ca, and Ca + K) provide less information and are presented elsewhere (Gadley, 2005). In the first and second plots (Figs. F5, F6), the data spreads are consistently large with a similar data distribution for all stain combinations and no distinct pop-

F6. Lvvsv ± Lvvmv vs. Lvvhv ± Lvvw vs. shard texture plots, p. 15.

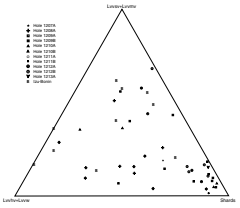

F7. Lvu vs. Lvy vs. platy texture plot, p. 16.

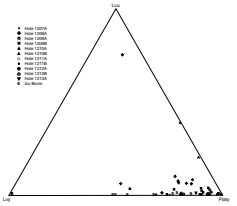

F8. Quantitative method of likeliness of correlation, p. 17.

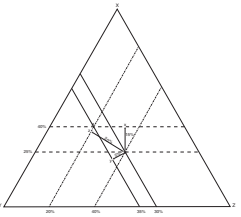

T4. Ash interval matrix correlations, p. 24.

ulations. Both of these plots illustrate the tendency for the samples from Site 1208 to be more vesiculated. The third plot (Fig. F7) shows the overall dominance of platy over Y- or U-shaped shards.

Ash Layer Correlations

The variability among the textural and compositional proportions of the ash beds shown in Figures F5, F6, and F7 and Table T3 suggests that these attributes could be used to "fingerprint" ash for detailed bed-by-bed correlation. First approximations of correlativity are provided by the age estimates (biostratigraphic and magnetostratigraphic) in Table T1. Initially the ash layers were correlated based on age and then quantified based on textural composition. Correlations between the ash layers of similar age within holes at a site as well as from site to site were evaluated (Table T4; Fig. F9). The shallowest three ash layers found in Holes 1212A and 1212B were the first to be evaluated using this technique because this series of ash beds appeared to be very similar in both holes based on lithology and magnetic susceptibility (as observed by K.M. Marsaglia and other shipboard scientists). Correlation tests for the three ash layers within Holes 1212A (Samples 198-1212A-2H-6, 77 cm; 3H-1, 92 cm; and 3H-2, 95 cm) and 1212B (Samples 198-1212B-2H-7, 65 cm; 3H-1, 144 cm; and 3H-3, 12 cm) are good to excellent (Table T4; Fig. F9). Furthermore, the correlation test for a pair of slightly older ash beds in these two holes (Samples 198-1212A-4H-4, 37 cm, and 198-1212B-4H-4, 58 cm) also rates as excellent. At Site 1209 ash layers similar in age to the two sets discussed above do not correlate as well compositionally, but these exhibit a poor compositional correlation between holes (1209A and 1209B). Sample 198-1207A-2H-4, 59 cm, shows a good correlation to Sample 198-1208A-5H-2, 1 cm. Samples 198-1209A-2H-6, 72 cm, and 2H-6, 85 cm, provide good correlations to Samples 198-1209B-3H-1, 129 cm, and 3H-2, 11 cm, and Sample 198-1209A-3H-1, 30 cm, is an excellent correlation to Sample 198-1209B-3H-3, 88 cm. Sample 198-1209A-3H-1, 30 cm, is also good correlation to its depositional counterparts, Samples 198-1209B-3H-3, 88 cm, 3H-4, 48 cm, and 3H-134, 4 cm. Samples 198-1209A-4H-3, 24 cm, and 4H-5, 55 cm, are good and excellent correlations to Samples 198-1209B-4H-6, 104 cm, and 5H-1, 110 cm, respectively. Although very similar in both age and depth, Samples 198-1210A-11H-1, 142 cm, and 198-1210B-10H-6, 42 cm, show only a moderate correlation.

The correlations in Figure F9 are not unique; to show this we also tested samples of different ages. A total of 113 tests of compositional/textural similarities were evaluated (Table T4). Of these, 19% showed excellent compositional similarity, 28% showed good compositional similarity, 27% showed moderate compositional similarity, and 26% showed poor compositional similarity. These percentages are similar to those generated for the age equivalence/correlations in Figure F9. Results for various sample pairs with excellent to good compositional/textural similarities are shown in Figure F10.

F9. Age-constrained correlations, p. 18.

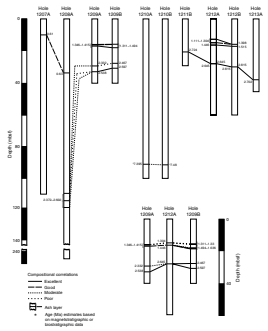

F10. Excellent and good compositional similarities, p. 19.

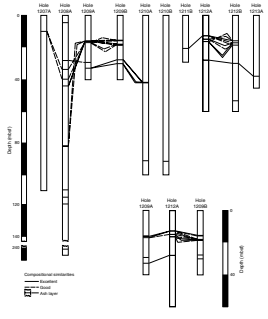

DISCUSSION

Ash Composition, Texture, and Provenance

The nonvesicular and blocky (Lvv) texture and black to brown color of some vitric clasts suggests that they are mafic to intermediate in

composition. A small percentage of these fragments (Table T1) could be attributed to magma mixing or, more likely, to incorporation of lithic fragments during eruptions. The range in the staining characteristics of the colorless glassy fragments likely reflects their range from more intermediate (Ca) to dacitic (Ca + K) to rhyolitic (K) compositions. Note that as shown in Table T3, there were only two cases where most of the fragments took only the Ca stain and many more where the majority took just the K stain. Most of the samples are mixtures of fragments with both Ca and K stain. Phenocryst assemblages in these ashes are also consistent with intermediate to felsic sources.

The ash textures observed in these samples are likely products of vesiculation of silicic magmas during Plinian to Phreatoplinian eruptions (Fisher and Schmincke, 1984; Heiken and Wohletz, 1985). Specific shapes of pyroclasts are dependent on the size, shape, and density of vesicles, which in turn reflect the magma composition, temperature, and volatile content just prior to eruption (Heiken and Wohletz, 1985). Shards can be the product of explosive disintegration of pumice during frothing or bubble coalescence (Heiken and Wohletz, 1985).

The above interpretation assumes that all the ash beds on Shatsky Rise are the distant fallout of large eruption plumes. An alternative source for submarine ash is the production of fines during abrasion of floating pumice rafts (Fisher and Schmincke, 1984). The presence of rounded pumice gravel-sized clasts in Shatsky ash-bearing units makes pumice comminution a viable source of ash. Unfortunately, we know of no studies comparing grain size or morphology of shards produced by this process as opposed to air fall processes; however, it is likely that pumice rafts would produce coarser material (Fisher and Schmincke, 1984). Based on data from Site 1208 (see below), we suspect that enrichment in vesiculated glassy fragments is also an indicator of pumice rafts.

Geographical considerations indicate several possible sources of ash delivered to Shatsky Rise and recovered during ODP Leg 198. First, airborne ash could have been transported from either the Japan or Kurile magmatic arc systems and pumice from eruptions in the Kurile arc. These were the major sources of pyroclastic debris at Site 810 that Natland (1993) considered, although both he and Cao et al. (1995), in a later study of northwestern Pacific DSDP and ODP sites, depicted the Kuroshio Current extending to Shatsky Rise from the region of the Izu-Bonin island arc. The Kuroshio Current, which passes across Shatsky Rise, is a known conduit of pumice rafts from the Mariana and Izu-Bonin magmatic arcs to the south (Lisitzin, 1972). The importance of this possible source may have been overlooked by Natland (1993) because the thick pumice deposits associated with the Sumisu Rift in the Izu-Bonin arc (Leg 126; Taylor, Fujioka, et al., 1990; Nishimura et al., 1991) had not yet been discovered (drilled) when Natland published his work. Thus, pumice and (abraded) ash derived from pumice rafts could have been transported to Shatsky Rise from the Izu-Bonin arc.

Although previous workers (e.g., Marsaglia, 1992) defined compositional modes for volcaniclastic sediments, including pumice-raft debris, along the length of the Japan and Izu-Bonin arcs, they did not use the pyroclast classification scheme outlined in this study. Therefore, we collected textural data from these samples and compared the Izu-Bonin (Leg 126) and Shatsky Rise (Leg 198) ash records. The Izu-Bonin samples, when plotted on the same ternary plots with Shatsky Rise samples (Figs. F5, F6, F7), have a higher vesiculated and lower shard proportion. The lower proportion of vesiculated fragments at Leg 198 sites could

possibly be due to the physical alteration of the ash grains during transport and subsequent deposition and reworking.

Correlation of Ash Beds among Shatsky High Sections

The above discussion of pyroclast generation and textural attributes implies that individual eruptions may produce characteristic ash deposits. When correlating across large areas, however, one must take into consideration possible eolian fractionation, whereby wind-transported ash is sorted by size and composition. This effect has mainly been called on to explain bulk changes in ash composition as related to the concentration of denser lithic fragments and crystals nearer the vent and the more distant transport of less dense siliceous glass (see discussion in Fisher and Schmincke, 1984). What we do not know is to what degree this process affects heterogeneous compositions of glassy fragments or pyroclast shapes. For the purposes of this discussion, therefore, we have assumed that these remain constant.

As might be expected, the correlations are best between ash beds in adjacent holes but less certain between sites, particularly those from different highs on Shatsky Rise. Part of the intersite differences may be related to possible thickness variations owing to variable sinking rates of particles, pelletization in the water column, and shallow current transport, as well as reworking by bottom currents and, once the ash is deposited, the impact of bioturbative mixing on preservation potential (Fisher and Schmincke, 1984). Some of the samples analyzed from Shatsky Rise were taken from ash-filled burrows.

As mentioned above, the vitric component population at Site 1208 is generally more vesicular; furthermore, the section at Site 1208 contains a significant number of isolated pumice clasts (Cores 198-1208A-10H through 19H) (Bralower, Premoli Silva, Malone, et al., 2002). Perhaps the more vesicular character of the ashes at Site 1208 is the product of localization of pumice raft-bearing currents. Deeper currents, however, must be responsible for creating the anomalously thick pile of sediment drift cored at this site. As the source of this drift might be in part the adjacent gully (Bralower, Premoli Silva, Malone, et al., 2002), there is also the possibility of duplicating the ash record by reworking. After deposition of primary fallout across the gully and drift topography, ash might then be eroded from the gully and transported onto the pile of sediment drift. We did not see any textural evidence for this phenomenon in the sand-sized fraction.

CONCLUSIONS

There appear to be two mechanisms for delivering tephra to Shatsky Rise: air fall from eruption clouds and ablation and sinking of floating pumice carried by ocean currents. The relative importance of these phenomena is likely to change across the rise, with the Central High being more prone to pumice events. The currents that formed the large drifts that contain the ash layers have likely modified the record of ash accumulation on the Central High. One possible source of pumice is the Izu-Bonin arc to the south, which is illustrated by the high vesiculated component present in both Izu-Bonin samples and Site 1208 samples, whereas the Japan and Kurile arcs, as Natland (1993) also concluded, are the likely sources of the airborne ash. Historically, ash correlation in the deep sea has been attempted using criteria such as color, thickness

isopachs, and chemical composition, as well as shard morphology. Herein we provide a scheme for fingerprinting and correlating ashes using shard morphology, as well as chemistry, by the glass color and stain information. It is reasonably inexpensive, and because it is petrographically based, it could also be used to correlate lithified tuffs. However, our results indicate that on Shatsky Rise, tephra correlation cannot be based on the compositional/textural data alone.

ACKNOWLEDGMENTS

We thank Tim Bralower, Debbie Thomas, and Dave Rea, who provided helpful suggestions on early versions of this paper that were incorporated into this final version. This research used samples, data, and funding provided by the Ocean Drilling Program (ODP). ODP is sponsored by the U.S. National Science Foundation (NSF) and participating countries under management of Joint Oceanographic Institutions (JOI), Inc. Helen Evans graciously allowed us access to unpublished magnetostratigraphic data.

REFERENCES

Bralower, T.J., Premoli Silva, I., Malone, M.J., et al., 2002. *Proc. ODP, Init. Repts.,* 198 [CD-ROM]. Available from: Ocean Drilling Program, Texas A&M University, College Station TX 77845-9547, USA.

Bray, J.R., 1974. Volcanism and glaciation during the past 40 millennia. *Nature (London, U.K.),* 252:679–680.

Bray, J.R., 1979. Neogene explosive volcanicity, temperature and glaciation. *Nature (London, U.K.),* 282:603–605.

Cande, S.C., and Kent, D.V., 1995. Revised calibration of the geomagnetic polarity timescale for the Late Cretaceous and Cenozoic. *J. Geophys. Res.,* 100:6093–6095.

Cao, L.-Q., Arculus, R.J., and McKelvey, B.C., 1995. Geochemistry and petrology of volcanic ashes recovered from Sites 881 through 884: a temporal record of Kamchatka and Kurile volcanism. *In* Rea, D.K., Basov, I.A., Scholl, D.W., and Allan, J.F. (Eds.), *Proc. ODP, Sci. Results,* 145: College Station, TX (Ocean Drilling Program), 345–381.

Dickinson, W.R., 1970. Interpreting detrital modes of graywacke and arkose. *J. Sediment. Petrol.,* 40:695–707.

Fisher, R.V., and Schmincke, H.-U., 1984. *Pyroclastic Rocks:* New York (Springer-Verlag).

Gadley, K.L., 2005. Petrography and correlation of Cenozoic ash layers recovered on Shatsky Rise, ODP Leg 198 [MS thesis]. California State Univ., Northridge.

Heiken, G., and Wohletz, K., 1985. *Volcanic Ash:* Berkeley (Univ. of California Press).

Ingersoll, R.V., Bullard, T.F., Ford, R.L., Grimm, J.P., Pickle, J.D., and Sares, S.W., 1984. The effect of grain size on detrital modes: a test of the Gazzi-Dickinson point-counting method. *J. Sediment. Petrol.,* 54:103–116.

Kennett, J.P., 1977. On explosive Cenozoic volcanism and climatic implications. *Science,* 196:1231–1234.

Kennett, J.P., McBirney, A.R., and Thunnell, R.C., 1977. Episodes of Cenozoic volcanism in the Circum-Pacific region. *J. Volcanol. Geotherm. Res.,* 2:145–163.

Lisitzin, A.P., 1972. Sedimentation in the world ocean. *Spec. Publ.—Soc. Econ. Paleontol. Mineral.,* 17.

Marsaglia, K.M., 1992. Petrography and provenance of volcaniclastic sands recovered from the Izu-Bonin arc, Leg 126. *In* Taylor, B., Fujioka, K., et al., *Proc. ODP, Sci. Results,* 126: College Station, TX (Ocean Drilling Program), 139–154.

Marsaglia, K.M., and Tazaki, K., 1992. Diagenetic trends in Leg 126 sandstones. *In* Taylor, B., Fujioka, K., et al., *Proc. ODP, Sci. Results,* 126: College Station, TX (Ocean Drilling Program), 125–138.

Natland, J.H., 1993. Volcanic ash and pumice at Shatsky Rise: sources, mechanisms of transport, and bearing on atmospheric circulation. *In* Natland, J.H., Storms, M.A., et al., *Proc. ODP, Sci. Results,* 132: College Station, TX (Ocean Drilling Program), 57–66.

Nishimura, A., Marsaglia, K.M., Rodolfo, K.S., Colella, A., Hiscott, R.N., Tazaki, K., Gill, J.B., Janecek, T., Firth, J., Isiminger-Kelso, M., Herman, Y., Taylor, R.N., Taylor, B., Fujioka, K., and Leg 126 Scientific Party, 1991. Pliocene–Quaternary submarine pumice deposits in the Sumisu rift area, Izu-Bonin arc. *In* Fisher, R.V., and Smith, G.A. (Eds.), *Sedimentation in Volcanic Settings*. Spec. Publ.—SEPM (Soc. Sediment. Geol.), 45:201–208.

Prueher, L.M., and Rea, D.K., 1998. Rapid onset of glacial conditions in the subarctic North Pacific region at 2.67 Ma: clues to causality. *Geology,* 26:1027–1030.

Sliter, W.V., and Brown, G.R., 1993. Shatsky Rise: seismic stratigraphy and sedimentary record of Pacific paleoceanography since the Early Cretaceous. *In* Natland, J.H., Storms, M.A., et al., *Proc. ODP, Sci. Results,* 132: College Station, TX (Ocean Drilling Program), 3–13.

Taylor, B., Fujioka, K., et al., 1990. *Proc. ODP, Init. Repts.,* 126: College Station, TX (Ocean Drilling Program).

Figure F1. Leg 198 site location map from Bralower, Premoli Silva, Malone, et al. (2002).

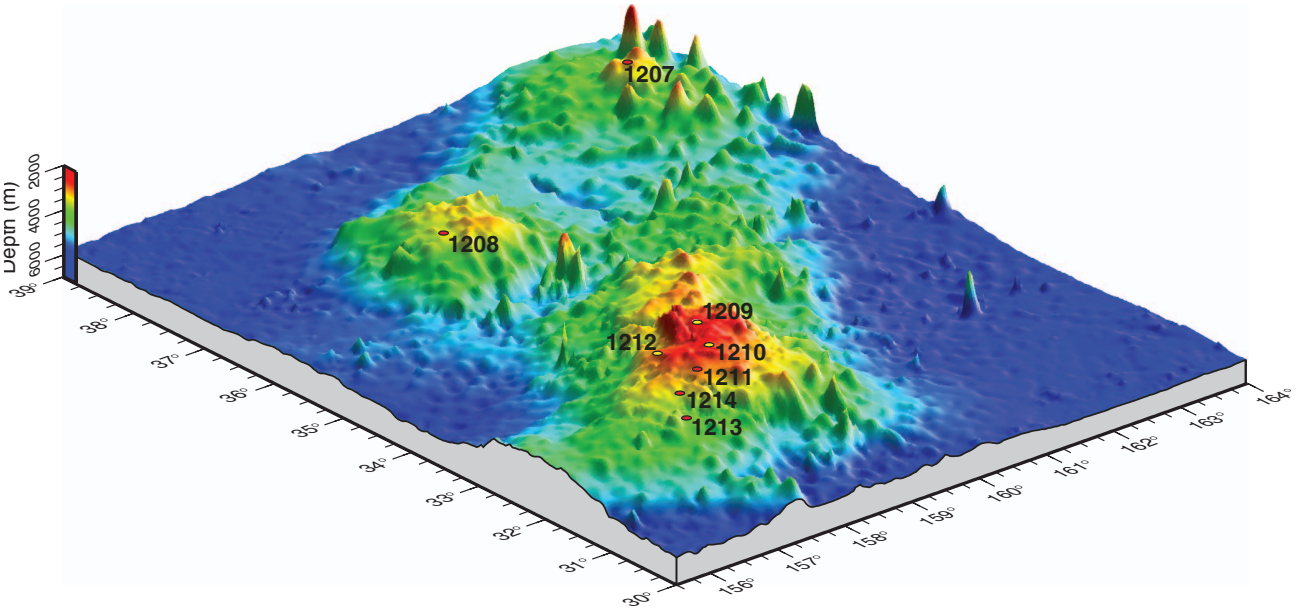

Figure F2. Stratigraphic columns and ash layer occurrence at Leg 198 sites indicating samples with sufficient sand-sized material for which compositional modes were determined in this study.

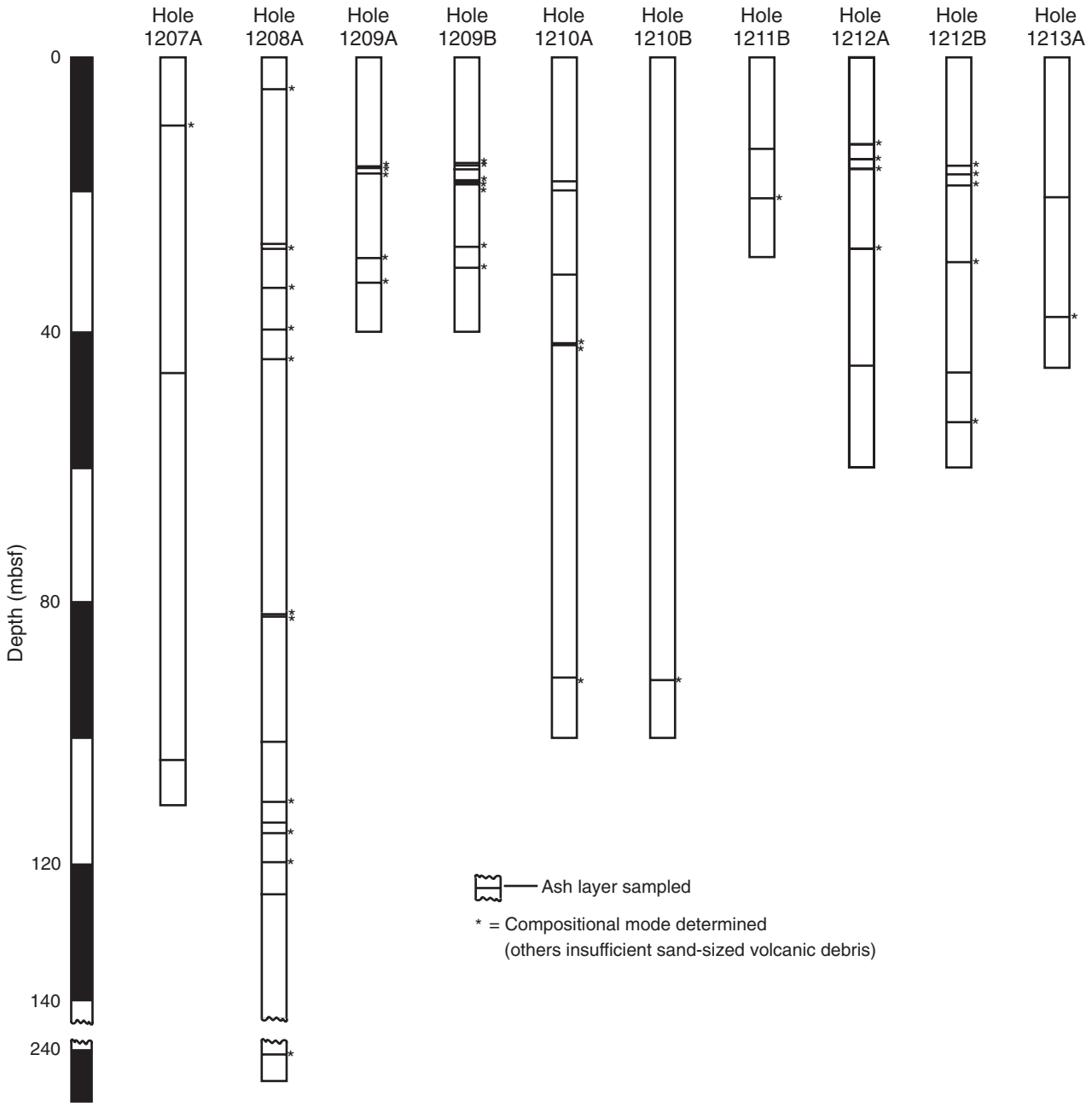

Figure F3. Pyroclast classification scheme developed for this study.

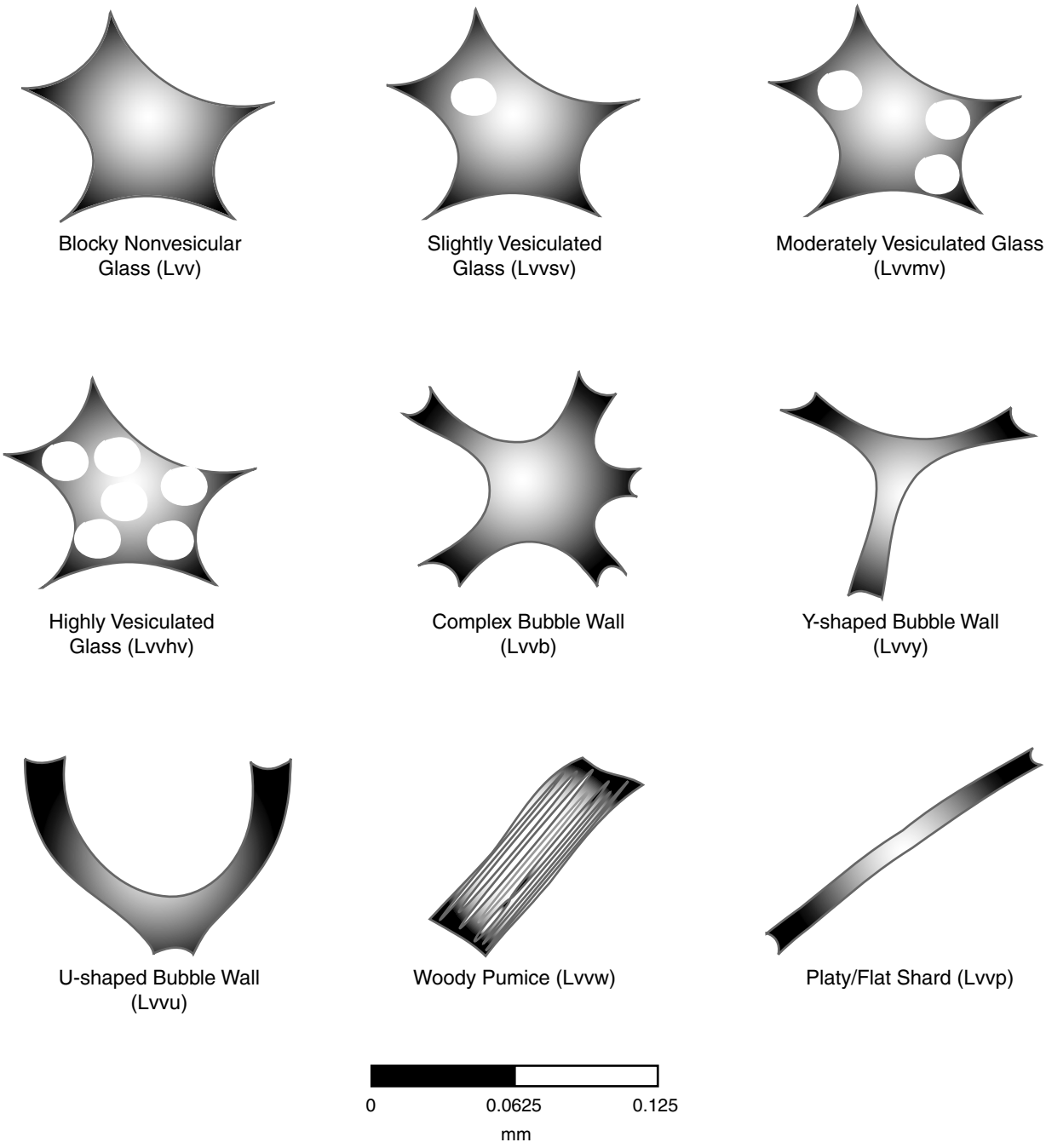

Figure F4. Total colorless glass components plotted according to stain (K vs. Ca vs. K + Ca).

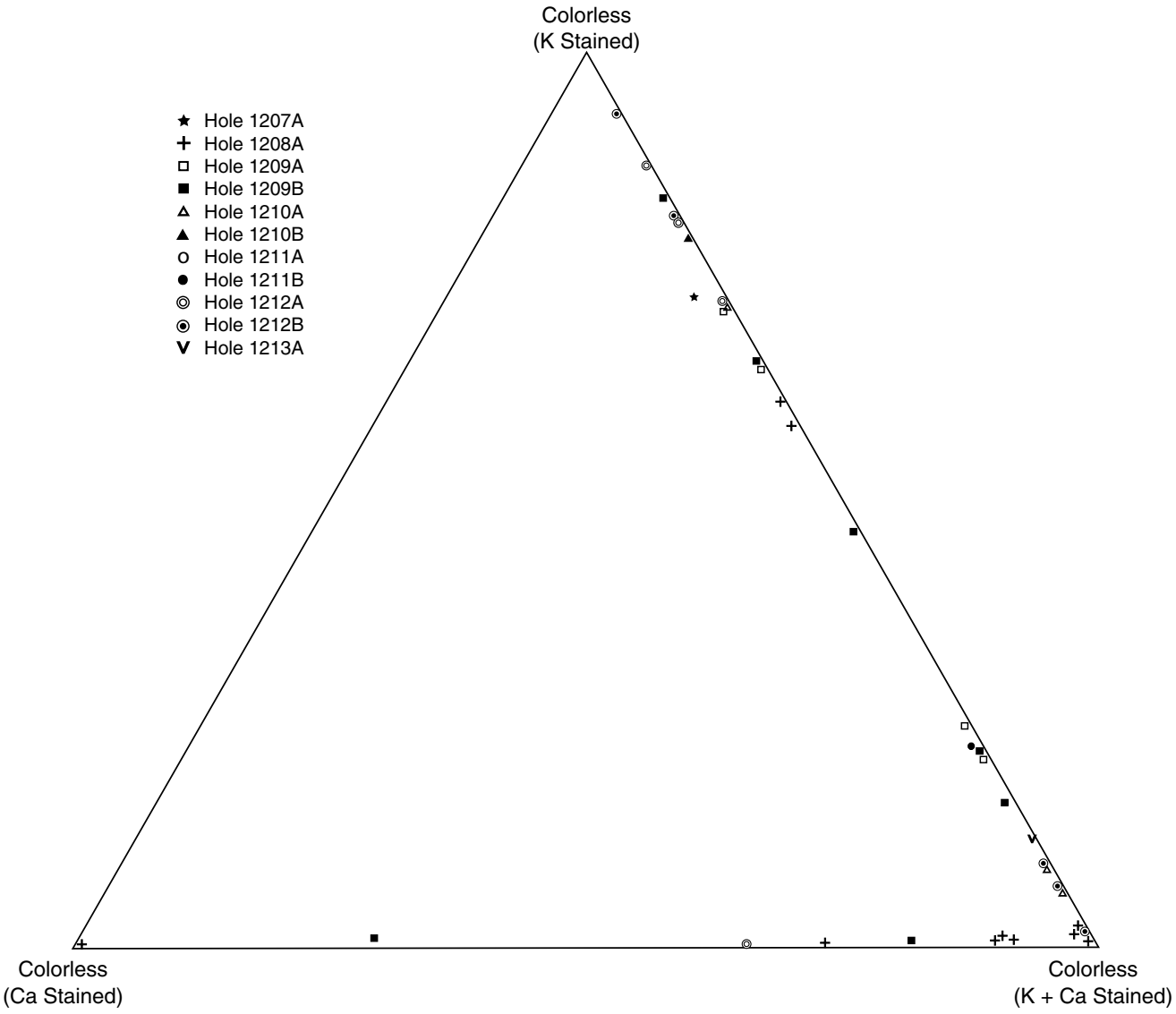

Figure F5. Plot of vesiculated vs. shards vs. blocky textures totaled for all stained colorless glassy fragments.

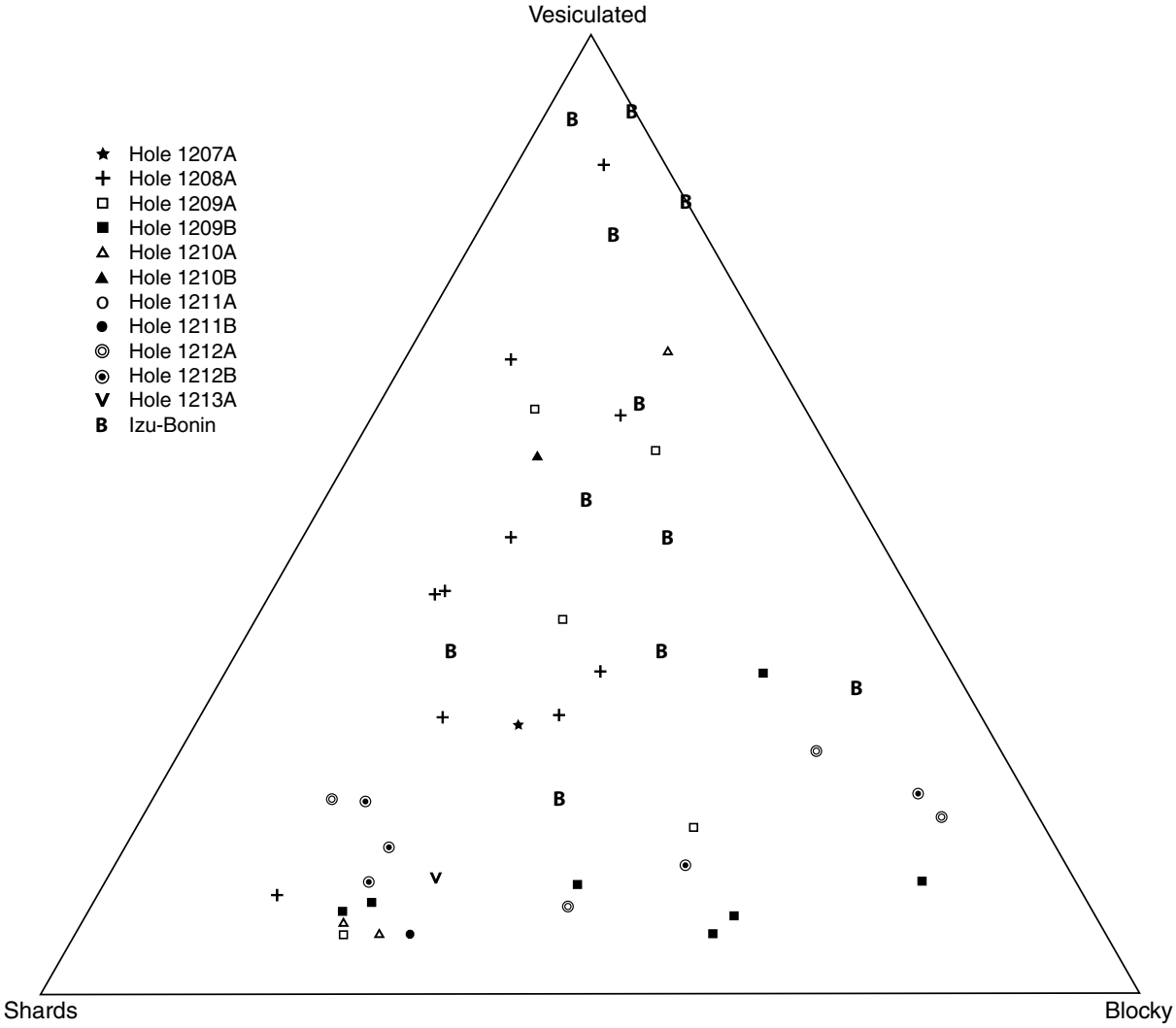

Figure F6. Plot of Lvvsv + Lvvmv vs. Lvvhv + Lvvw vs. shard textures totaled for all stained colorless glassy fragments.

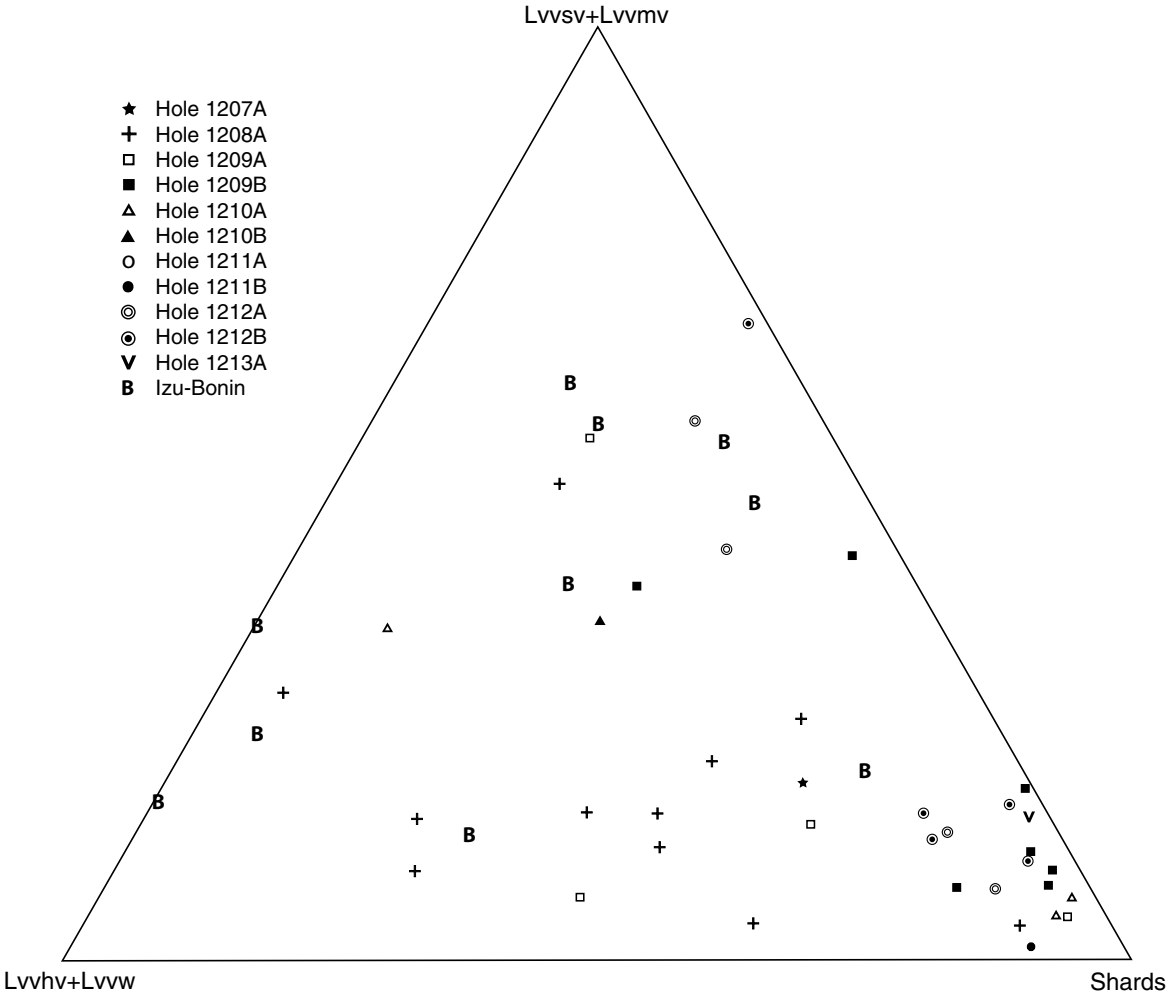

Figure F7. Plot of Lvu vs. Lvy vs. platy textures totaled for all stained colorless glassy fragments.

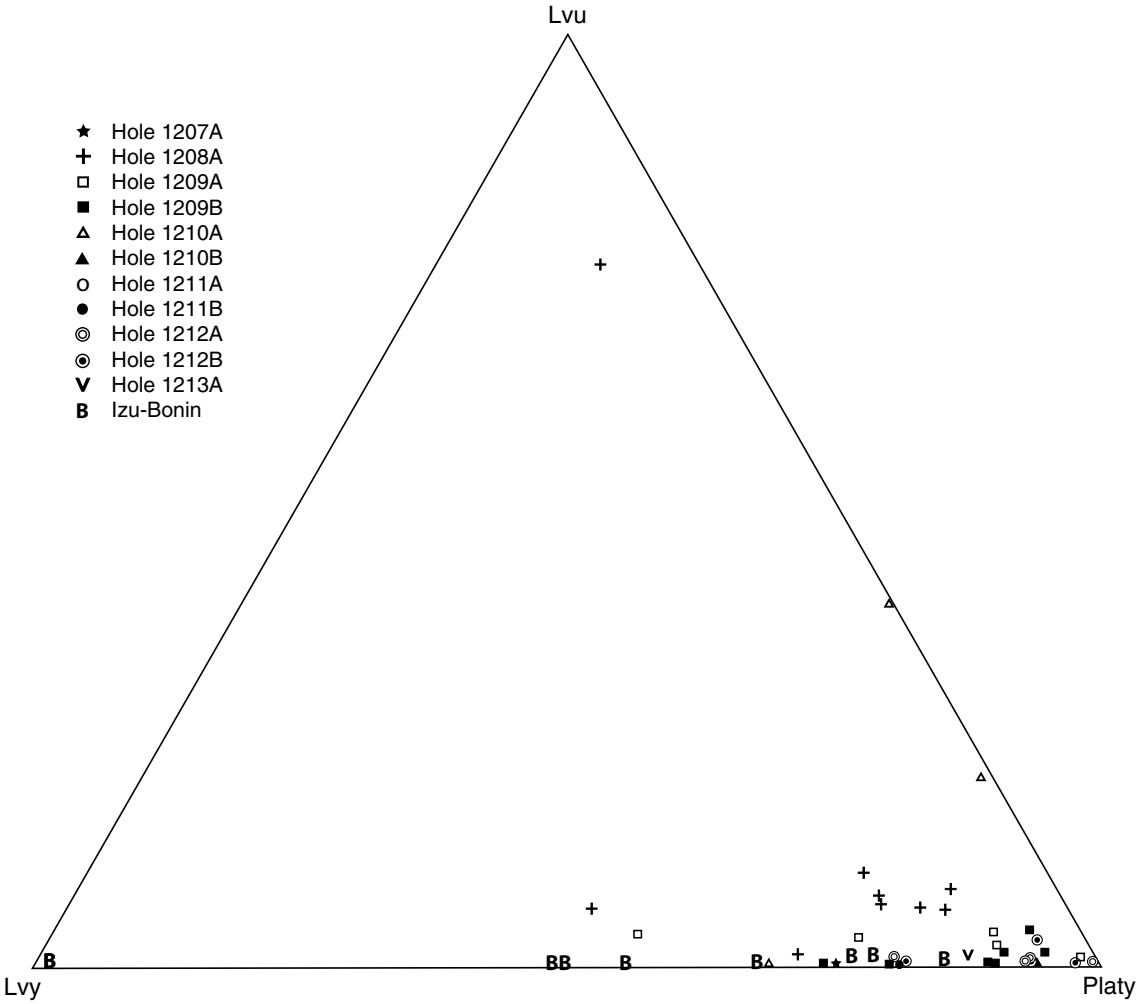

Figure F8. Schematic showing the quantitative method of likeliness of correlation. The percentage difference indicates the compositional "distance" between samples A and B in ternary space. The lesser of the three distances was chosen to represent the likeliness of correlation for a given plot in Table **T4,** p. 24.

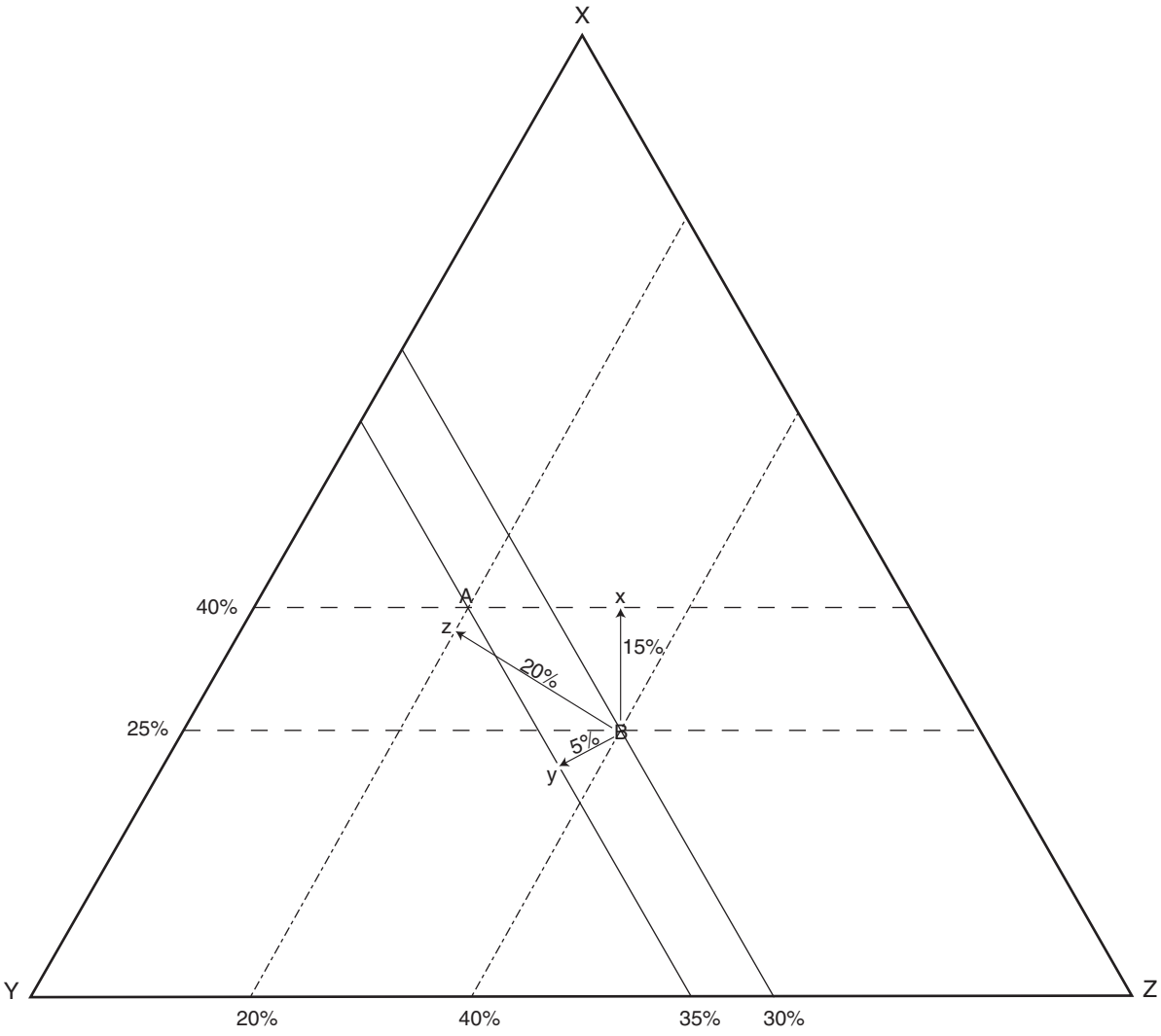

Figure F9. Compositional correlation chart showing age-constrained correlations tested in Table T4, p. 24. Quality of correlation is keyed to "Total Percentage" values in Table T4, p. 24. See text and Figure F8, p. 17, for explanation of correlation method.

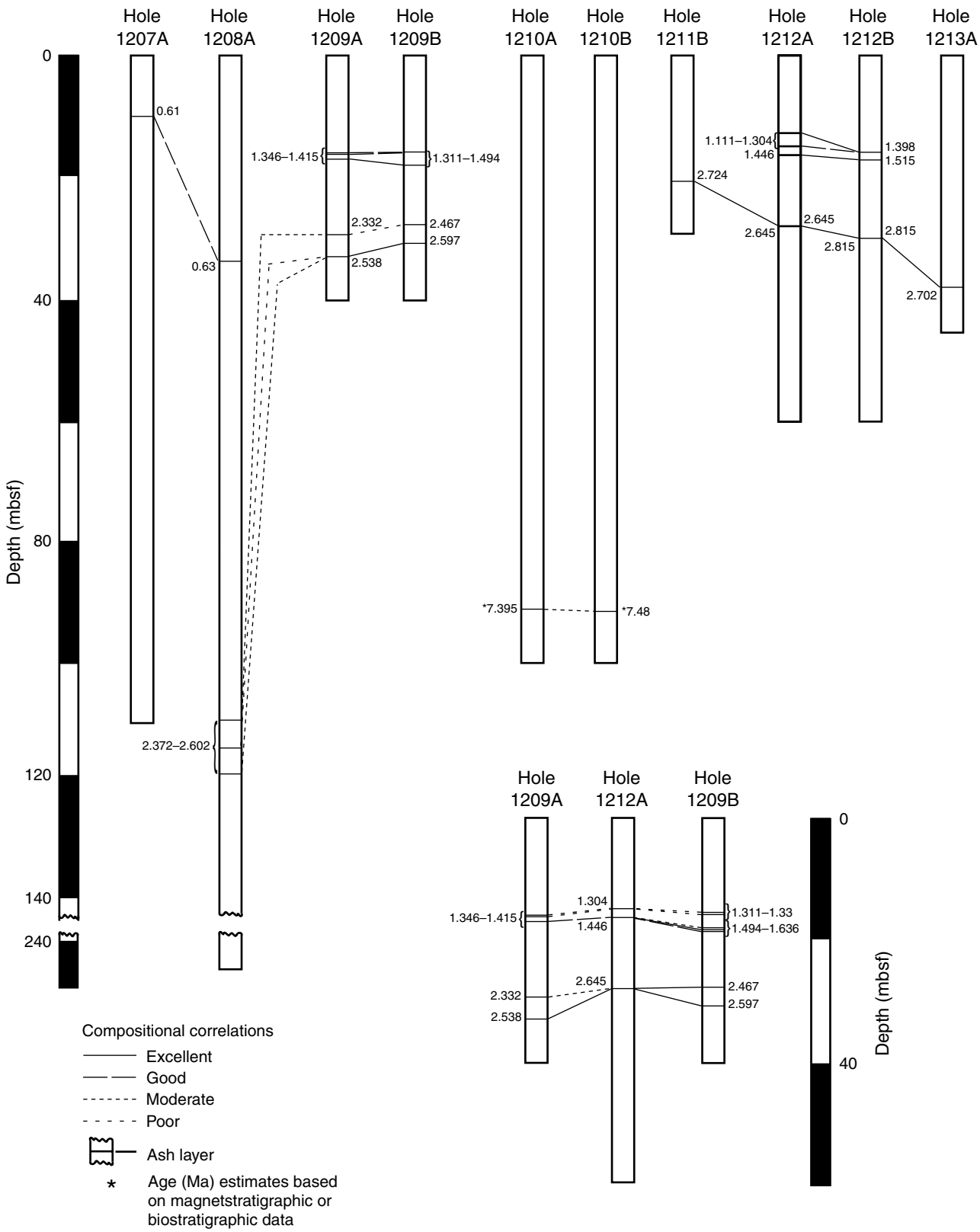

Figure F10. Chart showing excellent and good compositional similarities based on data in Table T4, p. 24. Degree of similarity is keyed to "Total Percentage" values in Table T4, p. 24. See text and Figure F8, p. 17, for explanation of correlation method. Note that moderate and poor correlations are not shown.

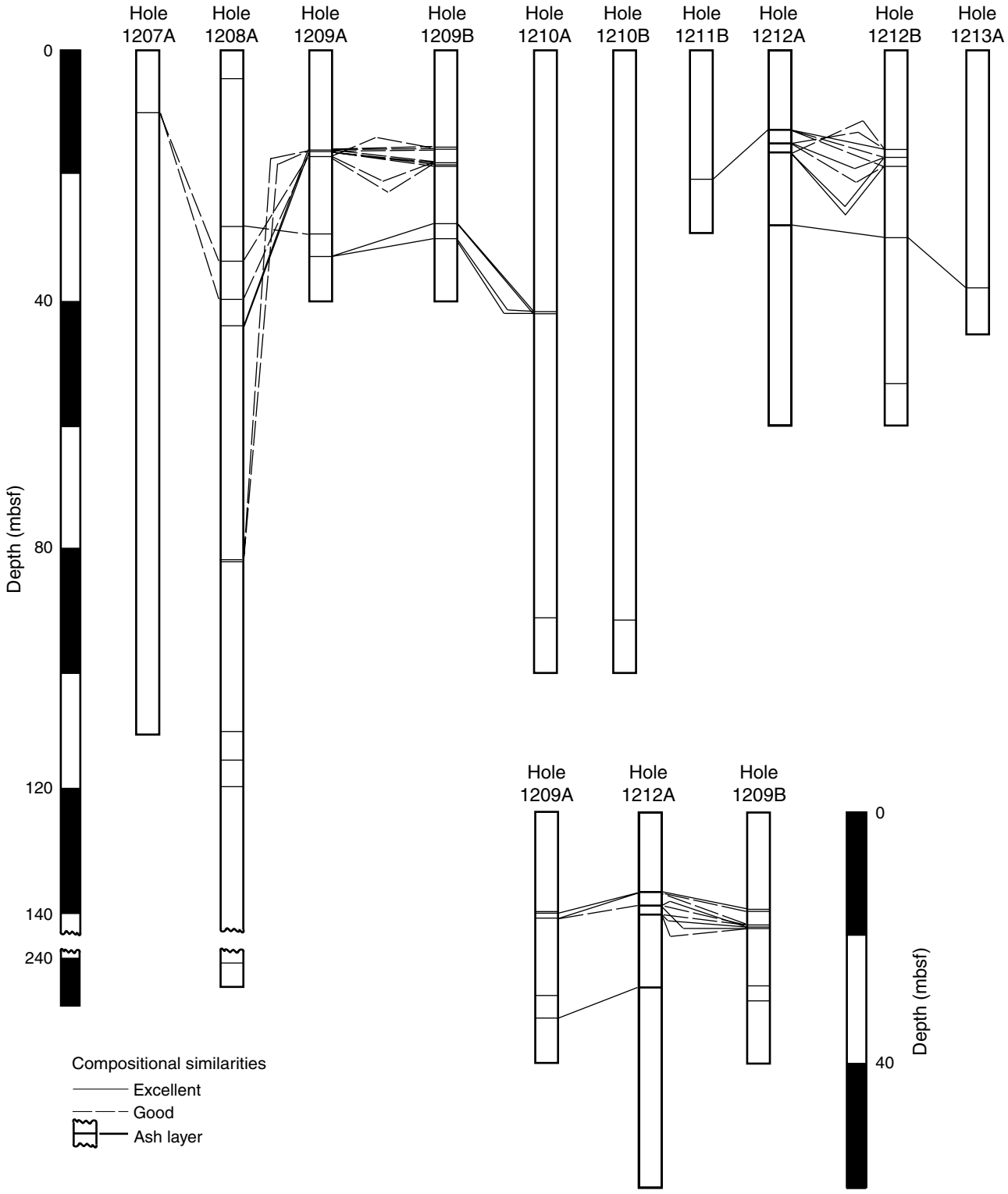

Table T1. Sample intervals and age estimates for all samples, with point count data for those samples petrographically analyzed. (This table is available in an **oversized format.**)

Table T2. Definitions of counted and recalculated parameters. (Continued on next page.)

Counted parameters:	
Lvv =	blocky nonvesicular glass
Lvvsv =	slightly vesiculated glass
Lvvmv =	moderately vesiculated glass
Lvvhv =	highly vesiculated glass
Lvvb =	complex bubble wall glass
Lvvy =	Y-shaped bubble wall glass
Lvvu =	U-shaped bubble wall glass
Lvvw =	woody pumice
Lvvp =	platy/flat shard
Q =	monocrystalline quartz
P =	plagioclase feldspar
Py =	pyroxene
A =	amphibole
D =	dense minerals
Biotite =	biotite mica
K-spar =	biotite mica
Shards =	Lvvp + Lvvy + Lvvu
Vesiculated =	Lvvsv + Lvvmv + Lvvhv + Lvvw
Blocky =	Lvv
Stained =	total fragments with K-stain or Ca-stain or both
K =	fragments with K-stain
Ca =	fragments with Ca-stain
K/Ca =	fragments with K-stain Ca-stain
Recalculated parameters:	
Unstained colorless =	[colorless vesiculated glass + colorless shards + colorless Lvvb] / [colorless vesiculated glass + colorless shards + colorless Lvvb + stained vesiculated glass + stained shards + stained Lvvb + colored vesiculated glass + colored shards + colored Lvvb] · 100
Stained colorless =	[stained vesiculated glass + stained shards + stained Lvvb] / [stained vesiculated glass + stained shards + stained Lvvb + colorless vesiculated glass + colorless shards + colorless Lvvb + colored vesiculated glass + colored shards + colored Lvvb] · 100
Colored =	[colored vesiculated glass + colored shards + colored Lvvb] / [colored vesiculated glass + colored shards + colored Lvvb + stained vesiculated glass + stained shards + stained Lvvb + colorless vesiculated glass + colorless shards + colorless Lvvb] · 100
K-stained =	[K-stained vesiculated glass + K-stained shards + K-stained Lvvb] / [K-stained vesiculated glass + K-stained shards + K-stained Lvvb + Ca-stained vesiculated glass + Ca-stained shards + Ca-stained Lvvb + K/Ca- vesiculated glass + K/Ca-shards + K/Ca-colorless Lvvb] · 100
Ca-stained =	[Ca-stained vesiculated glass + Ca-stained shards + Ca-stained Lvvb] / [Ca-stained vesiculated glass + Ca-stained shards + Ca-stained Lvvb + K-stained vesiculated glass + K-stained shards + K-stained Lvvb + K/Ca- vesiculated glass + K/Ca-shards + K/Ca-colorless Lvvb] · 100
K/Ca-stained =	[K/Ca-stained vesiculated glass + K/Ca-stained shards + K/Ca-stained Lvvb] / [K/Ca-stained vesiculated glass + K/Ca-stained shards + K/Ca-stained Lvvb + K-stained vesiculated glass + K-stained shards + K-stained Lvvb + Ca- vesiculated glass + Ca-shards + Ca-colorless Lvvb] · 100
Vesiculated stained =	[vesiculated stained] / [vesiculated stained + shards stained + blocky stained] · 100
Shards stained =	[shards stained] / [shards stained + vesiculated stained + blocky stained] · 100
Blocky stained =	[shards stained] / [shards stained + vesiculated stained + blocky stained] · 100
Vesiculated (K/Ca) =	[vesiculated (K/Ca)] / [vesiculated (K/Ca) + shards (K/Ca) + blocky (K/Ca)] · 100
Shards (K/Ca) =	[shards (K/Ca)] / [shards (K/Ca) + vesiculated (K/Ca) + blocky (K/Ca)] · 100
Blocky (K/Ca) =	[vesiculated (K/Ca)] / [vesiculated (K/Ca) + shards (K/Ca) + blocky (K/Ca)] · 100
Vesiculated (K) =	[vesiculated (K)] / [vesiculated (K) + shards (K) + blocky (K)] · 100
Shards (K) =	[shards (K)] / [shards (K) + vesiculated (K) + blocky (K)] · 100
Blocky (K) =	[vesiculated (K)] / [vesiculated (K) + shards (K) + blocky (K)] · 100
Vesiculated (Ca) =	[vesiculated (Ca)] / [vesiculated (Ca) + shards (Ca) + blocky (Ca)] · 100
Shards (Ca) =	[shards (Ca)] / [shards (Ca) + vesiculated (Ca) + blocky (Ca)] · 100
Blocky (Ca) =	[vesiculated (Ca)] / [vesiculated (Ca) + shards (Ca) + blocky (Ca)] · 100
Lvvsv/Lvvmv stained =	[Lvvsv/Lvvmv stained] / [Lvvsv/Lvvmv stained + Lvvhv/Lvvw stained + shards stained] · 100
Lvvhv/Lvvw stained =	[Lvvhv/Lvvw stained] / [Lvvhv/Lvvw stained + Lvvsv/Lvvmv stained + shards stained] · 100
Shards stained =	[shards stained] / [shards stained + Lvvsv/Lvvmv stained + Lvvhv/Lvvw stained] · 100
Lvvsv/Lvvmv (K/Ca) =	[Lvvsv/Lvvmv (K/Ca)] / [Lvvsv/Lvvmv (K/Ca) + Lvvhv/Lvvw (K/Ca) + shards (K/Ca)] · 100
Lvvhv/Lvvw (K/Ca) =	[Lvvhv/Lvvw (K/Ca)] / [Lvvhv/Lvvw (K/Ca) + Lvvsv/Lvvmv (K/Ca) + shards (K/Ca)] · 100
Shards (K/Ca) =	[shards (K/Ca)] / [shards (K/Ca) + Lvvsv/Lvvmv (K/Ca) + Lvvhv/Lvvw (K/Ca)] · 100
Lvvsv/Lvvmv (K) =	[Lvvsv/Lvvmv (K)] / [Lvvsv/Lvvmv (K) + Lvvhv/Lvvw (K) + shards (K)] · 100
Lvvhv/Lvvw (K) =	[Lvvhv/Lvvw (K)] / [Lvvhv/Lvvw (K) + Lvvsv/Lvvmv (K) + shards (K)] · 100
Shards (K) =	[shards (K)] / [shards (K) + Lvvsv/Lvvmv (K) + Lvvhv/Lvvw (K)] · 100
Lvvsv/Lvvmv (Ca) =	[Lvvsv/Lvvmv (Ca)] / [Lvvsv/Lvvmv (Ca) + Lvvhv/Lvvw (Ca) + shards (Ca)] · 100
Lvvhv/Lvvw (Ca) =	[Lvvhv/Lvvw (Ca)] / [Lvvhv/Lvvw (Ca) + Lvvsv/Lvvmv (Ca) + shards (Ca)] · 100
Shards (Ca) =	[shards (Ca)] / [shards (Ca) + Lvvsv/Lvvmv (Ca) + Lvvhv/Lvvw (Ca)] · 100
Lvvu stained =	[Lvvu stained] / [Lvvu stained + Lvvy stained + platy stained] · 100
Lvvy stained =	[Lvvy stained] / [Lvvy stained + Lvvu stained + platy stained] · 100
Platy stained =	[Platy stained] / [Platy stained + Lvvy stained + Lvvu stained] · 100
Lvvu (K/Ca) =	[Lvvu (K/Ca)] / [Lvvu (K/Ca) + Lvvy (K/Ca) + platy (K/Ca)] · 100
Lvy (K/Ca) =	[Lvvy (K/Ca)] / [Lvvy (K/Ca) + Lvvu (K/Ca) + platy (K/Ca)] · 100
Platy (K/Ca) =	[Platy (K/Ca)] / [Platy (K/Ca) + Lvvy (K/Ca) + Lvvu (K/Ca)] · 100
Lvvu (K) =	[Lvvu (K)] / [Lvvu (K) + Lvvy (K) + platy (K)] · 100
Lvvy (K) =	[Lvvy (K)] / [Lvvy (K) + Lvvu (K) + platy (K)] · 100
Platy (K) =	[Platy (K)] / [Platy (K) + Lvvy (K) + Lvvu (K)] · 100

Table T2 (continued).

Lvvu (Ca) =	[Lvvu (Ca)] / [Lvvu (Ca) + Lvvy (Ca) + platy (Ca)] · 100
Lvvy (Ca) =	[Lvvy (Ca)] / [Lvvy (Ca) + Lvvu (Ca) + platy (Ca)] · 100
Platy (K/Ca) =	[Platy (Ca)] / [Platy (Ca) + Lvvy (Ca) + Lvvu (Ca)] · 100

Table T3. Recalculated parameters for samples petrographically analyzed. (This table is available in an **oversized format.**)

Table T4. Correlation of matrices for selected ash intervals using minimum percent difference on ternary plot (mpdtp). (**See table notes.** Continued on next two pages.)

Correlation: Hole, core, section, interval (cm)	Vesiculated shards blocky				Lvvsv/Lvvmv Lvvhv/Lvvw shards				Lvu Lvy platy				Total mpdtp	Total common ternary plots	Average mpdtp
	Stained	K-stained	Ca-stained	K- and Ca-stained	Stained	K-stained	Ca-stained	K- and Ca-stained	Stained	K-stained	Ca-stained	K- and Ca-stained			
198-															
1207A-2H-4, 99, to 1208A-4H-4, 62	7	15	19	8.5	7	22	18	8	NA	30	0	5	139.5	11	12.68
1207A-2H-4, 99, to 1208A-5H-2, 1	1	1	NA	2.5	3	0.5	NA	6	1	31	NA	3	49	9	5.44
1207A-2H-4, 99, to 1208A-5H-6, 30	10	NA	2.5	0	3.5	NA	9.5	3.5	0.5	NA	3	2.5	35	9	3.89
1208A-4H-4, 62, to 1209A-2H-6, 72	5.5	NA	9	1	24.5	NA	20	21	3.5	NA	9.5	2.5	96.5	9	10.72
1208A-4H-4, 62, to 1209A-2H-6, 72	1	36	NA	8	NA	10	NA	22	4	0	NA	3.5	84.5	8	10.56
1208A-4H-4, 62, to 1209A-3H-1, 30	15.5	8	NA	15	5	15	NA	7	1	0	NA	3	69.5	9	7.72
1208A-4H-4, 62, to 1209A-4H-3, 24	1.5	15.5	NA	2.5	0.5	8.5	NA	1	4	0	NA	0	33.5	9	3.72
1208A-4H-4, 62, to 1209A-4H-5, 55	2	4	NA	2	24	6	NA	25	3	0	NA	1.5	67.5	9	7.50
1208A-5H-2, 1, to 1209A-2H-6, 72	4.5	NA	NA	3	11	NA	NA	13	2	NA	NA	1	34.5	6	5.75
1208A-5H-2, 1, to 1209A-2H-6, 85	14.5	23	NA	9.5	NA	13	NA	21	3	0	NA	0	84	8	10.50
1208A-5H-2, 1, to 1209A-3H-1, 30	7.5	13	NA	3.5	5	5.5	NA	7	0.5	0	NA	0.5	42.5	9	4.72
1208A-5H-2, 1, to 1209A-4H-3, 24	5.5	3.5	NA	20	4.5	14.5	NA	3	2.5	0	NA	3.5	57	9	6.33
1208A-5H-2, 1, to 1209A-4H-5, 55	8.5	3.5	NA	14	14	10.5	NA	10.5	1.5	0	NA	4	66.5	9	7.39
1208A-5H-6, 30, to 1209A-2H-6, 72	0.5	NA	12.5	3.5	4	NA	0.5	2.5	0	NA	1.5	0	25	9	2.78
1208A-5H-6, 30, to 1209A-2H-6, 85	4.5	NA	NA	1	NA	NA	NA	1.5	4	NA	NA	6	17	5	3.40
1208A-5H-6, 30, to 1209A-3H-1, 30	2	NA	NA	10	1	NA	NA	1	7	NA	NA	7.5	28.5	6	4.75
1208A-5H-6, 30, to 1209A-4H-3, 24	8	NA	NA	4	20	NA	NA	3.5	4	NA	NA	10.5	50	6	8.33
1208A-5H-6, 30, to 1209A-4H-5, 55	5.5	NA	NA	6	10	NA	NA	10.5	4	NA	NA	3	39	6	6.50
1208A-10H-2, 112, to 1209A-2H-6, 72	11	NA	NA	9	2.5	NA	NA	5	2.5	NA	NA	5.5	35.5	6	5.92
1208A-10H-2, 112, to 1209A-2H-6, 85	2	10	NA	3	4.5	NA	NA	8	2	0	NA	8	37.5	8	4.69
1208A-10H-2, 112, to 1209A-3H-1, 30	7	7	NA	11	10	10	NA	7	5	0	NA	5	62	9	6.89
1208A-10H-2, 115, to 1209A-2H-6, 72	9	NA	7	17	8	NA	0.5	8	13	NA	10	7.5	80	9	8.89
1208A-10H-2, 115, to 1209A-2H-6, 85	0.5	NA	NA	5	3	NA	NA	5.5	1	NA	NA	6.5	21.5	6	3.58
1208A-10H-2, 115, to 1209A-3H-1, 30	8	NA	NA	18	0.5	NA	NA	2.5	8	NA	NA	10	47	6	7.83
1208A-13H-2, 54, to 1209A-4H-3, 24	12	NA	NA	4	6	NA	NA	NA	3.5	NA	NA	6.5	32	5	6.40
1208A-13H-2, 54, to 1209A-4H-5, 55	8.5	NA	NA	6	16.5	NA	NA	18	5	NA	NA	1	55	6	9.17
1208A-13H-5, 83, to 1209A-4H-3, 24	12	14	NA	5	16	21	NA	NA	5.5	NA	NA	9	82.5	7	11.79
1208A-13H-5, 83, to 1209A-4H-5, 55	9	35	NA	5	7	12	NA	8	1	NA	NA	2	79	8	9.88
1208A-14H-2, 53, to 1209A-4H-3, 24	NA	NA	NA	16	14	NA	NA	NA	6	NA	NA	11	47	4	11.75
1208A-14H-2, 53, to 1209A-4H-5, 55	NA	NA	NA	8	11	NA	NA	8	7	NA	NA	4	38	5	7.60
1209A-2H-6, 72, to 1209B-3H-1, 129	12	NA	0.5	14	1.5	NA	5	1	2	NA	9.5	0	45.5	9	5.06
1209A-2H-6, 72, to 1209B-3H-2, 11	6	NA	7.5	3	2	NA	5	5	1.5	NA	6	2.5	38.5	9	4.28
1209A-2H-6, 72, to 1209B-3H-3, 88	3	NA	NA	5	5	NA	NA	2	4	NA	NA	NA	19	5	3.80
1209A-2H-6, 72, to 1209B-3H-4, 48	6	NA	NA	8.5	12	NA	NA	11	3.5	NA	NA	2	43	6	7.17
1209A-2H-6, 72, to 1209B-3H-4, 134	19	NA	NA	3	7	NA	NA	1.5	3.5	NA	NA	2	36	6	6.00
1209A-2H-6, 85, to 1209B-3H-1, 129	21	NA	NA	21	NA	NA	NA	4	2.5	NA	NA	1	49.5	5	9.90
1209A-2H-6, 85, to 1209B-3H-2, 11	9	NA	NA	3.5	NA	NA	NA	7.5	2.5	NA	NA	2.5	25	5	5.00
1209A-2H-6, 85, to 1209B-3H-3, 88	12	NA	NA	1	NA	NA	NA	1	4	NA	NA	NA	18	4	4.50
1209A-2H-6, 85, to 1209B-3H-4, 48	7	NA	NA	10	NA	NA	NA	1	4	NA	NA	3	25	5	5.00
1209A-2H-6, 85, to 1209B-3H-4, 134	11	NA	NA	4	NA	NA	NA	5	2	NA	NA	3	25	5	5.00

Table T4 (continued).

Correlation: Hole, core, section, interval (cm)	Vesiculated shards blocky				Lvvsv/Lvvmv Lvvhv/Lvvw shards				Lvu Lvy platy				Total mpdtp	Total common ternary plots	Average mpdtp
	Stained	K-stained	Ca-stained	K- and Ca-stained	Stained	K-stained	Ca-stained	K- and Ca-stained	Stained	K-stained	Ca-stained	K- and Ca-stained			
1209A-3H-1, 30, to 1209B-3H-1, 129	6	NA	NA	3	7.5	15	NA	6	1	1.5	NA	1	41	8	5.13
1209A-3H-1, 30, to 1209B-3H-2, 11	9.5	NA	NA	16	7.5	NA	NA	11	0.5	NA	NA	3	47.5	6	7.92
1209A-3H-1, 30, to 1209B-3H-3, 88	7	8.5	NA	7	3	4	NA	5	1	0	NA	NA	35.5	8	4.44
1209A-3H-1, 30, to 1209B-3H-4, 48	2	1.5	NA	8	4	12	NA	2.5	0	0.5	NA	2.5	33	9	3.67
1209A-3H-1, 30, to 1209B-3H-4, 134	5.5	3	NA	10	10.5	22	NA	8	1	0	NA	3	63	9	7.00
1209A-4H-3, 24, to 1209B-4H-6, 104	17.5	1	NA	32	22	7	NA	21	1	0	NA	5.5	107	9	11.89
1209A-4H-3, 24, to 1209B-5H-1, 110	3	18	NA	4	19	5	NA	22	4	0	NA	0	75	9	8.33
1209A-4H-5, 55, to 1209B-4H-6, 104	3	1	NA	1.5	4	4	NA	3	2	0	NA	1.5	20	9	2.22
1209A-4H-5, 55, to 1209B-5H-1, 110	1.5	1	NA	1	1	2.5	NA	2	2	0	NA	7	18	9	2.00
1209B-4H-6, 104, to 1210A-5H-6, 102	2	10	NA	0	4	2	NA	3	4	0	NA	4.5	29.5	9	3.28
1209B-4H-6, 104, to 1210A-5H-6, 106	1.5	10	NA	2	1.5	2	NA	3	4	0	NA	5	29	9	3.22
1209B-5H-1, 110, to 1210A-5H-6, 102	1	10	NA	1	2	3	NA	1.5	0	0	NA	1	19.5	9	2.17
1209B-5H-1, 110, to 1210A-5H-6, 106	1	2.5	NA	1	0	3	NA	1.5	4.5	0	NA	0.5	14	9	1.56
1210A-11H-1, 142, to 1210B-10H-6, 42	6	2.5	NA	19	0.5	7	NA	19	5	5	NA	0	64	9	7.11
1211B-3H-4, 111, to 1212A-4H-4, 37	3	2	NA	2.5	0.5	3	NA	0	0	1	NA	1	13	9	1.44
1212A-2H-6, 77, to 1212B-2H-7, 65	0.5	NA	NA	1	0.5	NA	NA	1	2	NA	NA	1	6	6	1.00
1212A-2H-6, 77, to 1212B-3H-1, 144	5	NA	NA	4	2	NA	NA	9	1	NA	NA	0.5	21.5	6	3.58
1212A-2H-6, 77, to 1212B-3H-3, 12	1	NA	NA	6	8	NA	NA	14	0.5	NA	NA	0	29.5	6	4.92
1212A-3H-1, 92, to 1212B-2H-7, 65	5.5	1	NA	5	4	8	NA	9	0.5	0	NA	3.5	36.5	9	4.06
1212A-3H-1, 92, to 1212B-3H-1, 144	6	3	NA	9	4	4	NA	1	0.5	0	NA	0.5	28	9	3.11
1212A-3H-1, 92, to 1212B-3H-3, 12	4	7	NA	3	9	7	NA	4	0.5	NA	NA	0.5	35	8	4.38
1212A-3H-2, 95, to 1212B-2H-7, 65	1.5	8	NA	5	0.5	6	NA	12	2	0	NA	1	36	9	4.00
1212A-3H-2, 95, to 1212B-3H-1, 144	5.5	5	NA	9	0	1.5	NA	3	0	0	NA	0	24	9	2.67
1212A-3H-2, 95, to 1212B-3H-3, 12	1	1	NA	6	0	1.5	NA	1	0.5	NA	NA	0	11	8	1.38
1212A-4H-4, 37, to 1212B-4H-4, 58	2.5	1	NA	4	2	5	NA	3	0	1	NA	1.5	20	9	2.22
1212A-4H-4, 37, to 1213A-5R-2, 39	3	2.5	NA	8.5	1	5	NA	3	1	1	NA	0.5	25.5	9	2.83
1212B-4H-4, 58, to 1213A-5R-2, 39	0.5	3.5	NA	1	2.5	9.5	NA	5	1	0	NA	0.5	23.5	9	2.61
1208A-10H-2, 112, to 1208A-13H-2, 54	0.5	NA	NA	2	17	NA	NA	17.5	0.5	NA	NA	2	39.5	6	6.58
1208A-10H-2, 112, to 1208A-13H-5, 83	1	18	NA	3	8	4	NA	8.5	2	NA	NA	1	45.5	8	5.69
1208A-10H-2, 112, to 1208A-14H-2, 53	18	NA	NA	16	12	NA	NA	12	4	NA	NA	2.5	64.5	6	10.75
1208A-10H-2, 115, to 1208A-13H-2, 54	6.5	NA	NA	9	6.5	NA	NA	5	2	NA	NA	4.5	33.5	6	5.58
1208A-10H-2, 115, to 1208A-13H-5, 83	5.5	NA	32	10	0.5	NA	40	5	0.5	NA	NA	1	94.5	8	11.81
1208A-10H-2, 115, to 1208A-14H-2, 53	8	NA	18	11	4	NA	14	1	8	NA	NA	0.5	64.5	8	8.06
1208A-5H-2, 1, to 1212A-2H-6, 77	7.5	NA	NA	NA	8.5	NA	NA	0	0.5	NA	NA	3	19.5	5	3.90
1208A-5H-2, 1, to 1212A-3H-1, 92	4	1.5	NA	NA	2	NA	NA	6.5	0	0	NA	3.5	17.5	7	2.50
1208A-5H-2, 1, to 1212A-3H-2, 95	10	10.5	NA	NA	6	NA	NA	12	1.5	0	NA	3.5	43.5	7	6.21
1208A-5H-6, 30, to 1212A-2H-6, 77	2	NA	12	2	2	NA	8.5	1	2	NA	1.5	4	35	9	3.89
1208A-5H-6, 30, to 1212A-3H-1, 92	16	NA	NA	9	1.5	2.5	NA	21	8	NA	NA	4.5	62.5	7	8.93
1208A-5H-6, 30, to 1212A-3H-2, 95	24	NA	NA	12.5	11	8.5	NA	28	8	NA	NA	10.5	102.5	7	14.64
1208A-13H-2, 54, to 1212A-4H-4, 37	5	NA	NA	1	13	NA	NA	21	6.5	NA	NA	6	52.5	6	8.75

Table T4 (continued).

Correlation: Hole, core, section, interval (cm)	Vesiculated shards blocky				Lvvsv/Lvvmv Lvvhv/Lvvw shards				Lvu Lvy platy				Total mpdtp	Total common ternary plots	Average mpdtp
	Stained	K-stained	Ca-stained	K- and Ca-stained	Stained	K-stained	Ca-stained	K- and Ca-stained	Stained	K-stained	Ca-stained	K- and Ca-stained			
1208A-13H-5, 83, to 1212A-4H-4, 37	4	34	NA	1	4	12	NA	11	9	NA	NA	9	84	8	10.50
1208A-14H-2, 53, to 1212A-4H-4, 37	9.5	NA	NA	13	8	NA	NA	14.5	10	NA	NA	11	66	6	11.00
1208A-27H-1, 114, to 1210A-11H-1, 142	0	1	NA	3	18.5	33	NA	1	17	15	NA	7	95.5	9	10.61
1208A-27H-1, 114, to 1210B-10H-6, 42	5	3.5	NA	9	1.5	40	NA	1.5	7	0	NA	7	74.5	9	8.28
1208A-27H-1, 114, to 1212B-7-1, 49	2	0	NA	1	14	NA	NA	13	7	NA	NA	7	44	7	6.29
1209A-4H-3, 24, to 1212A-4H-4, 37	16	19.5	NA	6	13.5	6	NA	32.5	3.5	1	NA	0	98	10	9.80
1209A-4H-5, 55, to 1212A-4H-4, 37	3.5	1	NA	2.5	2.5	0.5	NA	3.5	2.5	0.5	NA	2	18.5	9	2.06
1209A-2H-6, 72, to 1212A-4H-4, 37	12	NA	7.5	5.5	7	NA	6	9	2.5	NA	3.5	2.5	55.5	9	6.17
1209A-2H-6, 72, to 1212A-3H-1, 92	16.5	NA	NA	12.5	5	NA	NA	16	3.5	NA	NA	2.5	56	6	9.33
1209A-2H-6, 72, to 1212A-3H-2, 95	24.5	NA	NA	15.5	15.5	NA	NA	11	3.5	NA	NA	2.5	72.5	6	12.08
1209A-2H-6, 85, to 1212A-2H-6, 72	2	NA	NA	0.5	NA	NA	NA	5.5	3	NA	NA	3	14	5	2.80
1209A-2H-6, 85, to 1212A-3H-1, 92	7.5	0.5	NA	6.5	NA	19.5	NA	27.5	4	0	NA	3	68.5	9	7.61
1209A-2H-6, 85, to 1212A-3H-2, 95	15.5	7	NA	9.5	NA	10	NA	22.5	4	0	NA	3	71.5	8	8.94
1209A-3H-1, 30, to 1212A-2H-6, 72	2.5	NA	NA	3	1	NA	NA	2.5	0	NA	NA	2.5	11.5	6	1.92
1209A-3H-1, 30, to 1212A-3H-1, 92	7.5	2	NA	6	7	4	NA	7	0	0	NA	2.5	36	9	4.00
1209A-3H-1, 30, to 1212A-3H-2, 95	15.5	4.5	NA	6	10	10	NA	11.5	0	0	NA	2.5	60	9	6.67
1209B-3H-1, 129, to 1212A-2H-6, 77	8.5	NA	0.5	11.5	2	NA	1.5	1.5	0.5	NA	1	2	29	9	3.22
1209B-3H-1, 129, to 1212A-3H-1, 92	14	29	NA	3.5	3.5	18	NA	7.5	1	1	NA	2	79.5	9	8.83
1209B-3H-1, 129, to 1212A-3H-2, 95	7.5	20	NA	4	1	12	NA	9.5	1.5	1	NA	1.5	58	9	6.44
1209B-3H-2, 11, to 1212A-2H-6, 77	7	NA	1	2.5	5.5	NA	1	12.5	1	NA	4.5	NA	35	8	4.38
1209B-3H-2, 11, to 1212A-3H-1, 92	17	NA	NA	12.5	12	NA	NA	4	0.5	NA	NA	NA	46	5	9.20
1209B-3H-2, 11, to 1212A-3H-2, 95	13	NA	NA	12.5	8	NA	NA	1.5	0	NA	NA	NA	35	5	7.00
1209B-3H-3, 88, to 1212A-2H-6, 77	13.5	NA	NA	0	0.5	NA	NA	6.5	0.5	NA	NA	0	21	6	3.50
1209B-3H-3, 88, to 1212A-3H-1, 92	0.5	1.5	NA	3.5	12	17.5	NA	0	0	0	NA	0	35	9	3.89
1209B-3H-3, 88, to 1212A-3H-2, 95	14.5	6	NA	3.5	7	12.5	NA	3.5	0	0	NA	0	47	9	5.22
1209B-3H-4, 48, to 1212A-2H-6, 77	13.5	NA	NA	12	15.5	NA	NA	8.5	0.5	NA	NA	0	50	6	8.33
1209B-3H-4, 48, to 1212A-3H-1, 92	1	1	NA	3	4	4.5	NA	7.5	0	0	NA	0	21	9	2.33
1209B-3H-4, 48, to 1212A-3H-2, 95	9	4	NA	1	3.5	10.5	NA	0.5	0	0	NA	0	28.5	9	3.17
1209B-3H-4, 134, to 1212A-2H-6, 77	8	NA	NA	18	6	NA	NA	3	1	NA	NA	0	36	6	6.00
1209B-3H-4, 134, to 1212A-3H-1, 92	3	4.5	NA	0.5	0.5	7.5	NA	6.5	1	0	NA	0	23.5	9	2.61
1209B-3H-4, 134, to 1212A-3H-2, 95	2	3	NA	4	6.5	6.5	NA	8.5	1	0	NA	NA	31.5	8	3.94
1211B-3H-4, 111, to 1212B-4H-4, 58	2	2.5	NA	3.5	4.5	4	NA	1.5	0	0	NA	0.5	18.5	9	2.06
1211B-3H-4, 111, to 1213A-5R-2, 39	1	0	NA	0.5	7	1.5	NA	5.5	1	0	NA	1	17.5	9	1.94

Notes: mpdtp = minimum percent difference on ternary plot. Total percentage is used to rank goodness of correlations shown in Figures **F9,** p.18, and **F10,** p.19. The average mpdtp was calculated by dividing the sum of the total mpdtp by the total number of ternary plots that the samples being correlated appeared on (i.e., "common" ternary plots). NA = not applicable.